Laser Physics, Vol. 12, No. 1, 2002, pp. 188–197.

Classical and Quantum Description of the Atomic Motion in Superradiant Light Scattering from Bose–Einstein Condensates

N. Piovella[1], M. Gatelli[1], L. Martinucci[1], R. Bonifacio[1], B. W. J. McNeil[2], and G. R. M. Robb[2]

[1] *Dipartimento di Fisica, Università Degli Studi di Milano, INFN & INFM, Via Celoria 16, Milano, I-20133 Italy*
e-mail: Nicola.Piovella@mi.infn.it

[2] *Department of Physics and Applied Physics, University of Strathclyde, Glasgow, Scotland, G4 0NG UK*

Received in final form July 1, 2001

Abstract—A theory of coherent light scattering from an elongated Bose–Einstein condensate exposed to an off-resonant laser beam is presented. The model describes the emission of two superradiant pulses along the sample's major axis simultaneous with the formation of a bidimensional atomic grating inside the sample, as was observed in a recent MIT experiment [Inouye, S. *et al.*, 1999, *Science*, **285**, 571]. The predictions of the semiclassical model, in which the atomic motion is treated classically, are compared with these of the quantum model, obtained including the quantum mechanical description of the atomic motion. In the quantum limit the superradiant regime becomes a sequential process, in which during each collective scattering atoms emit a π hyperbolic secant pulse and populate an adjacent momentum state.

1. INTRODUCTION

Recent experiments by Inouye *et al.* [1, 2] and Kozuma *et al.* [3] have demonstrated the formation of atomic matter waves in a cigar-shaped Bose–Einstein Condensate (BEC) pumped by an off-resonant laser beam, together with highly directional scattering of light along the major axis of the condensate. This emission has been interpreted in [1] as superradiant Rayleigh scattering, and successively investigated in [4] and [5] using a quantum theory based on a multi-mode extension of the Collective Atomic Recoil Laser (CARL) Hamiltonian model originally derived by Bonifacio *et al.* [6–8]. In particular, the semiclassical CARL model was extended in [9, 10] to include a quantum mechanical description of the center-of-mass motion of the atoms in the condensate. Whereas the analysis of [9, 10] is strictly limited to the linear regime and to the onset of the CARL instability starting from quantum fluctuations, an approximate description of the nonlinear effects due to momentum population depletion is contained in [4] and [5].

In a recent work [11] we have shown that the superradiant Rayleigh scattering from a BEC can be satisfactorily interpreted in terms of the CARL mechanism using a semiclassical model in the "mean-field" approximation, in which the rapid escape of the radiation from the condensate is modeled by a decay of the field amplitude at the rate $\kappa_c = c/2L$, where L is the sample length and c is the speed of light in vacuum. The main drawback of the semiclassical model is that, as it considers the center-of-mass motion of the atoms as classical, it cannot describe the discreteness of the recoil velocity, as has been instead observed in the MIT experiment [1]. For these reasons, the semiclassical CARL model was recently extended to include the quantum mechanical description of the center-of-mass motion of the atoms [12]. The basic result is that the quantization of the atomic motion becomes important when the average recoil momentum is comparable to $\hbar\mathbf{q}$ (where $\mathbf{q} = \mathbf{k}_2 - \mathbf{k}_1$ is the difference between the incident and the scattered wave vectors), i.e., the recoil momentum gained by the atom trading a photon via absorption and stimulated emission between the incident and scattered waves. In this limit, the quantum CARL equations reduce to the Maxwell–Bloch equations for two momentum levels [13]. The superradiant (SR) regime occurs for large radiation losses, i.e., $\kappa > 1$, where $\kappa = \kappa_c/\omega_r\rho$ is the field decay rate in units of the collective recoil bandwidth, $\omega_r\rho$, where $\omega_r = \hbar|\mathbf{q}|^2/2m_a$ is the recoil frequency, m_a is the atomic mass and ρ is the dimensionless CARL parameter [6], interpretable as the average number of photons scattered per atom. In the SR regime, the atomic motion becomes quantized when $\rho < \sqrt{2\kappa}$, whereas the semiclassical SR regime of [11] is obtained in the opposite limit. In [12] it has been shown that, in the quantum limit, a sequential superradiant scattering occurs, in which, during each process, the atoms emit a π hyperbolic secant pulse and populate an adjacent momentum level, as has been observed in the MIT experiment [1].

In this paper, we review the semiclassical and quantum theories describing the SR light scattering from a BEC, comparing the predictions of the two models with the MIT experiment [1]. The paper is organized as follows. In Section 2 we describe the bidimensional semiclassical CARL model and we obtain the semiclassical SR solution. In Section 3 we extend the semiclassical model including a quantum mechanical description of

the atomic motion in BECs. In Section 4 we discuss the quantum effects in the SR instability, whereas in Section 5 we describe analytically and numerically the nonlinear evolution of the average light intensity and atomic momentum in the sequential SR regime. Finally, in Section 6 we compare the theoretical results with the MIT experiment. Conclusions are drawn in Section 7.

2. SEMICLASSICAL BIDIMENSIONAL MODEL

The model described here is bidimensional and semiclassical. We represent the cigar-shaped atomic sample as an ellipsoid with length L and diameter W, where $L \gg W$ as shown in Fig. 1. The sample is exposed to a classical plane wave radiation electric field $\mathbf{E}_0(y, t) = \hat{x}\mathscr{E}_0\cos(k_2 y - \omega_2 t)$, polarized along the $\hat{x}$ axis and propagating along the $\hat{y}$ axis, with $\mathscr{E}_0$ real and constant and $\omega_2 = ck_2$. We assume that, due to the elongated geometry of the atomic sample, the scattering along the positive and negative direction of the $\hat{z}$ axis dominates over that in other directions, as has been explicitly discussed in [4], where a full multi-mode theory has shown that mode competition results in light scattering only within the geometric angle W/L. Hence, we assume that the scattered radiation consists of two oppositely directed radiation pulses propagating along the $\hat{z}$ axis, with electric fields polarized as the incident field:

$$\mathbf{E}(z, t) = (\hat{x}/2)[\mathscr{E}_1(z, t)e^{i(k_1 z - \omega_1 t)} + \mathscr{E}_2(z, t)e^{-i(k_1 z + \omega_1 t)} + \text{c.c}], \quad (1)$$

where $\mathscr{E}_{1,2}(z, t)$ are slowly varying complex amplitudes and $\omega_1 = ck_1 \approx \omega_2$. The atomic sample is described as a collisionless gas of atoms, each with two internal energy levels. The internal evolution of each atom is described by the density matrix elements ρ_{mn} (m, n = 1, 2) for the lower, (1), and upper, (2), levels. The off-diagonal elements $\rho_{12} = \rho_{21}^*$ describe the dipole moment induced by the radiation fields via the relation $\mathbf{d} = \hat{x}\mu(\rho_{12} + \text{c.c.})$, where μ is the dipole matrix element. The diagonal elements ρ_{11} and ρ_{22} describe the probability of an atom being in the lower or in the upper level, respectively. The off-diagonal elements may be described conveniently as a sum of three polarization waves:

$$\rho_{12} = (1/2)[S_0(z, t)e^{ik_2(y - ct)} + S_1(z, t)e^{ik_1(z - ct)} + S_2(z, t)e^{-ik_1(z + ct)}], \quad (2)$$

where $S_n(z, t)$ (n = 0, 1, 2) are slowly varying complex functions. The dipole moment of each atom contributes to the macroscopic polarization of the atomic sample described by $\mathbf{P} = n(\mathbf{x})\mathbf{d}$, where $n(\mathbf{x})$ is the atomic density. This polarization is a source for the radiation field

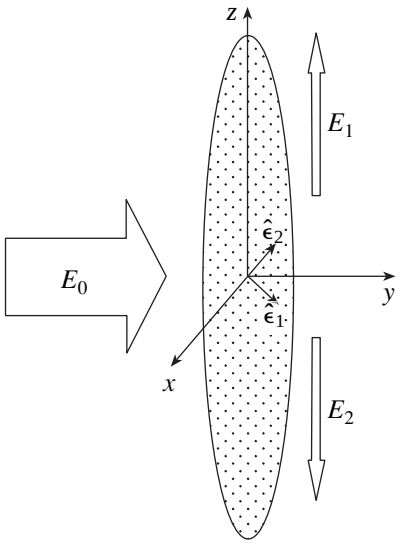

Fig. 1. The geometry of the scattering experiment. The filled ellipsoid, representing the atomic condensate with dimensions L and W, is illuminated with a single off-resonant laser beam of electric field E_0 polarized along the $\hat{x}$ axis and propagating along the $\hat{y}$ axis. The geometry favors the emission of two oppositely directed superradiant pulses E_1 and E_2 along the major axis L of the condensate. Also shown are the two recoil directions along the unit vectors $\hat{\epsilon}_{1,2}$.

via Maxwell's wave equation which yields, in the usual slowly varying envelope approximation,

$$\left(\frac{\partial\mathscr{E}_1}{\partial t} + c\frac{\partial\mathscr{E}_1}{\partial z}\right)e^{ik_1 z} + \left(\frac{\partial\mathscr{E}_2}{\partial t} - c\frac{\partial\mathscr{E}_2}{\partial z}\right)e^{-ik_1 z} = \frac{i\omega\mu}{2\epsilon_0}n(\mathbf{x})\{S_0 e^{ik_2 y - i\Delta_{21}t} + S_1 e^{ik_1 z} + S_2 e^{-ik_1 z}\}, \quad (3)$$

where we have neglected the terms proportional to $e^{\pm 2i\omega t}$ ("rotating wave" approximation), $\Delta_{21} = \omega_2 - \omega_1$ and, where possible, we have set $\omega_1 \approx \omega_2 \equiv \omega$. We assume that the atomic sample can be described as a collection of N point particles with positions $\mathbf{x}_j$, so that $n(\mathbf{x}) = \sum_{j=1}^{N}\delta^{(3)}(\mathbf{x} - \mathbf{x}_j)$. Multiplying both sides by $e^{\mp ik_1 z}$ and integrating over the $\hat{z}$ axis from $z - \Delta z/2$ to $z + \Delta z/2$, where $\Delta z = \pi/k_1$, Eq. (3) yields

$$\left(\frac{\partial\mathscr{E}_{1,2}}{\partial t} \pm c\frac{\partial\mathscr{E}_{1,2}}{\partial z}\right)\Delta z = \frac{i\omega\mu}{2\epsilon_0}\sum_{j=1}^{N}\{S_0 e^{i(k_2 y \mp k_1 z_j) - i\Delta_{21}t} + S_{1,2} + S_{2,1}e^{\mp 2ik_1 z_j}\}\delta(x - x_j)\delta(y - y_j), \quad (4)$$

where the upper sign corresponds to the first subscript and we have assumed the field amplitudes $\mathscr{E}_{1,2}$ spatially slowly varying over Δz. Assuming also that $\mathscr{E}_{1,2}$ are

independent of x and y, we can integrate on the plane (x, y) over the section $A = \pi(W/2)^2$ of the condensate, so that Eq. (4) becomes

$$\left(\frac{\partial \mathscr{E}_{1,2}}{\partial t} \pm c\frac{\partial \mathscr{E}_{1,2}}{\partial z}\right) = \frac{i\omega\mu n_a}{2\epsilon_0}\langle S_0 e^{i(k_2 y \mp k_1 z) - i\Delta_{21}t} + S_{1,2} + S_{2,1} e^{\mp 2ik_1 z}\rangle, \tag{5}$$

where $n_a = N/A\Delta z$ is the average density and $\langle..\rangle = (1/N)\sum_{j=1}^{N}(..)_j$. In this model the atomic center-of mass motion is treated classically, with each atom described as a point particle with a given position and momentum. The radiation fields drive the center-of-mass motion of the atoms via the force

$$\mathbf{F} = \left(0, \mathbf{d}\frac{\partial(\mathbf{E}_0 + \mathbf{E})}{\partial y}, \mathbf{d}\frac{\partial(\mathbf{E}_0 + \mathbf{E})}{\partial z}\right).$$

Neglecting the fast-varying temporal terms, the equations for the center-of-mass momentum components are

$$\frac{dp_y}{dt} = i(k\mu\mathscr{E}_0/4)[S_0^* + S_1^* e^{i(k_2 y - k_1 z) - i\Delta_{21}t} + S_2^* e^{i(k_2 y + k_1 z) - i\Delta_{21}t} - \text{c.c.}], \tag{6}$$

$$\frac{dp_z}{dt} = i(k\mu/4)\{S_1^*\mathscr{E}_1 - S_2^*\mathscr{E}_2 + S_2^*\mathscr{E}_1 e^{2ik_1 z} - S_1^*\mathscr{E}_2 e^{-2ik_1 z} + S_0^* e^{i\Delta_{21}t}[\mathscr{E}_1 e^{-i(k_2 y - k_1 z)} - \mathscr{E}_2 e^{-i(k_2 y + k_1 z)}] - \text{c.c.}\}. \tag{7}$$

We assume that the detuning $\Delta_0 = \omega - \omega_0$ between the optical fields and the atomic resonance is much larger than the natural linewidth of the atomic transition, γ, so that the atoms always remain in their lower internal energy states ($\rho_{11} \approx 1$ and $\rho_{22} \approx 0$). Moreover, assuming that the scattering time scale is much longer than the relaxation time γ^{-1}, we can adiabatically eliminate the atomic polarizations, i.e., $S_n = i(\mu/\hbar)\mathscr{E}_n/(\gamma/2 + i\Delta_0) \approx \Omega_n/\Delta_0$, where $\Omega_n = \mu\mathscr{E}_n/\hbar$ is the Rabi frequency for the field nth and $n = 0, 1, 2$. With these approximations, Eqs. (6) and (7) yield

$$\frac{dp_y}{dt} = -i\hbar k(\Omega_0/4\Delta_0) \times [\tilde{\Omega}_1 e^{i(k_1 z - k_2 y)} - \tilde{\Omega}_2^* e^{i(k_1 z + k_2 y)} - \text{c.c.}], \tag{8}$$

$$\frac{dp_z}{dt} = i\hbar k(\Omega_0/4\Delta_0) \times [\tilde{\Omega}_1 e^{i(k_1 z - k_2 y)} + \tilde{\Omega}_2^* e^{i(k_1 z + k_2 y)} - \text{c.c.}] + i(\hbar k/2\Delta_0)[\tilde{\Omega}_1\tilde{\Omega}_2^* e^{2ik_1 z} - \text{c.c.}], \tag{9}$$

where $\tilde{\Omega}_{1,2} = \Omega_{1,2} e^{i\Delta_{21}t}$. It is seen that the interference between the pump and the scattered fields forms two bidimensional pendulum potentials, $V_{1,2}(y, z) \propto |\mathscr{E}_0\mathscr{E}_{1,2}|\cos[\mathbf{q}_{1,2}\cdot\mathbf{x} \pm \phi_{1,2}]$, in the plane $(\hat{y}, \hat{z})$, where $\mathbf{q}_{1,2} = k_2\hat{y} \mp k_1\hat{z} \approx q\hat{\epsilon}_{1,2}$ (where $q = \sqrt{2}(\omega/c)$ and $\hat{\epsilon}_{1,2} = (\hat{y} \mp \hat{z})/\sqrt{2}$ are unit vectors) and $\phi_{1,2}$ are the phases of the complex amplitudes $\mathscr{E}_{1,2}$. A weaker 1D pendulum potential $V_3(z) \propto |\mathscr{E}_1\mathscr{E}_2|\cos[2k_1 z + \phi_1 - \phi_2]$ forms along the $\hat{z}$ axis due to the interference of the two counterpropagating scattered fields. If the pump intensity is large enough, we can assume $\mathscr{E}_0 \gg \mathscr{E}_{1,2}$ and neglect the potential V_3. Equations (8), (9), and (5) are conveniently written in the following dimensionless form [6]:

$$\frac{d\theta_j^{(1,2)}}{d\tau} = \bar{p}_j^{(1,2)}, \tag{10}$$

$$\frac{d\bar{p}_j^{(1,2)}}{d\tau} = [\tilde{A}_{1,2} e^{-i\theta_j^{(1,2)}} + \text{c.c}], \tag{11}$$

$$\frac{\partial\tilde{A}_{1,2}}{\partial\tau} \pm \frac{\partial\tilde{A}_{1,2}}{\partial\xi} = \langle e^{i\theta^{(1,2)}}\rangle + i\delta\tilde{A}_{1,2}, \tag{12}$$

where $j = 1, \ldots, N'$ and $N' = N/2$, $\theta_j^{(1,2)} = k_2 y_j \mp k_1 z_j \approx \mathbf{q}_{1,2}\mathbf{x}$, $\bar{p}_j^{(1,2)} = (p_{yj} \mp p_{zj})/\hbar k\rho \approx (2/\hbar q\rho)\mathbf{p}_j\hat{\epsilon}_{1,2}$, $A_{1,2} = -i(\epsilon_0/\hbar\omega n_s\rho)^{1/2}\mathscr{E}_{1,2}$ (where $n_s = n_a/2$) and $\tilde{A}_{1,2} = A_{1,2}e^{i\delta\tau}$ are dimensionless atomic position, atomic momentum and field amplitude variables, respectively. The dimensionless time and space coordinates, $\tau = \omega_r\rho t$ and $\xi = \omega_r\rho(z/c)$, and detuning, $\delta = \Delta_{2,1}/\omega_r\rho$, are scaled in terms of the collective recoil bandwidth, $\rho\omega_r$, where $\omega_r = \hbar k^2/m_a$ is the recoil frequency and $\rho = (\Omega_0/2\Delta_0)^{2/3}(\omega\mu^2 n_s/\hbar\epsilon_0\omega_r^2)^{1/3}$ is the collective CARL parameter [6, 7]. In Eq. (12) the average is defined as $\langle f(\theta^{(1,2)}, \bar{p}^{(1,2)})\rangle = (1/N')\sum_{j=1}^{N'} f(\theta_j^{(1,2)}, \bar{p}_j^{(1,2)})$. At $\tau = 0$, the atoms are assumed to be randomly distributed in position with zero momentum and, in the absence of any injected probe field, the emission starts from fluctuations. In this simple model the two scattered modes are uncoupled and symmetric, and we assume the atomic medium as made up of two independent classes of $N' = N/2$ atoms described by the variables $(\theta_j^{(1)}, \bar{p}_j^{(1)})$ and $(\theta_j^{(2)}, \bar{p}_j^{(2)})$, respectively. This is purely a mathematical and numerical convenience and imposes a decoupling of ensemble (1) from field (2) and vice versa. In reality, of course, there is nothing to prevent each individual atom emitting photons successively into either mode 1 or 2, so coupling to both modes. Although this coupling is not very relevant in the classical regime, it is however important in the quantum

regime and has been observed as a quantization in the momenta distribution of the atoms in the MIT experiment [1]. An atomic momentum has a value determined by the discrete number of recoil events it has experienced (photons scattered) with each mode. For each field (1, 2) individually, Eqs. (10)–(12) are formally identical to those which describe pulse propagation in a high-gain Free Electron Laser (FEL) [14]. It is well known that these equations admit a self-similar solution of the form $A_{1,2}(\xi, \tau) = \pm\xi\mathcal{A}(u)$, where $u = \sqrt{|\xi|}(\tau \mp \xi)$ and $\mathcal{A}(u)$ is the solution of a set of ordinary differential equations [15]. This self-similar solution describes SR emission of radiation pulses whose duration decreases in proportion to the fourth root of the peak intensity. The pulse shape of the first peak can be approximated by a hyperbolic secant function, followed by some nonlinear "ringing," similar to that which occurs in superfluorescence from inverted two-level atoms [16].

A simpler model can be obtained by approximating the spatial derivative in the field equation (12) by a damping term [17], i.e.,

$$\frac{d\tilde{A}_{1,2}}{d\tau} = \langle e^{i\theta^{(1,2)}} \rangle + (i\delta - \kappa)\tilde{A}_{1,2}, \qquad (13)$$

where $\kappa = c/2L\omega_r\rho$ and L/c is the transit time of the photon along the major axis of the condensate. In this approximation, the finite interaction time due to the escape of radiation from the atomic sample is represented by an incoherent decay of the field amplitude in the sample at a rate $c/2L$, half the inverse of the radiation "lifetime" in the atomic sample. A more general treatment where the radiation is scattered in a direction making an angle ψ with respect to the $\hat{z}$ axis should give $\kappa \approx (c/2\omega_r\rho)[|\sin\psi|/W + |\cos\psi|/L]$. As $L \gg W$, the radiation is least strongly damped along the major axis of the sample.

An approximate solution to Eqs. (10), (11), and (13) can be found assuming $\kappa \gg 1$ and $\delta = 0$ and adiabatically eliminating the field variable, i.e., $A_{1,2} \approx \kappa^{-1}\langle\exp[i\theta^{(1,2)}]\rangle$. In this limit, the rate of change of the average scaled momentum is $(d/d\tau)\langle \bar{p}^{(1,2)} \rangle = 2\kappa|A_{1,2}|^2$. A third-order analysis of the equations in the mean-field limit above gives the following approximate solution:

$$|A_{1,2}|^2 \approx \frac{1}{2\kappa^2}\operatorname{sech}^2[(\tau - \tau_D)/\sqrt{2\kappa}] \qquad (14)$$

and

$$\langle \bar{p}^{(1,2)} \rangle \approx \sqrt{\frac{2}{\kappa}}\{1 + \tanh[(\tau - \tau_D)/\sqrt{2\kappa}]\}, \qquad (15)$$

where $\tau_D = -\sqrt{2\kappa}\ln(b_0/\sqrt{2})$ is the delay time of the peak and $b_0 = |\langle\exp[i\theta^{(1,2)}(0)]\rangle|$ is the initial bunching,

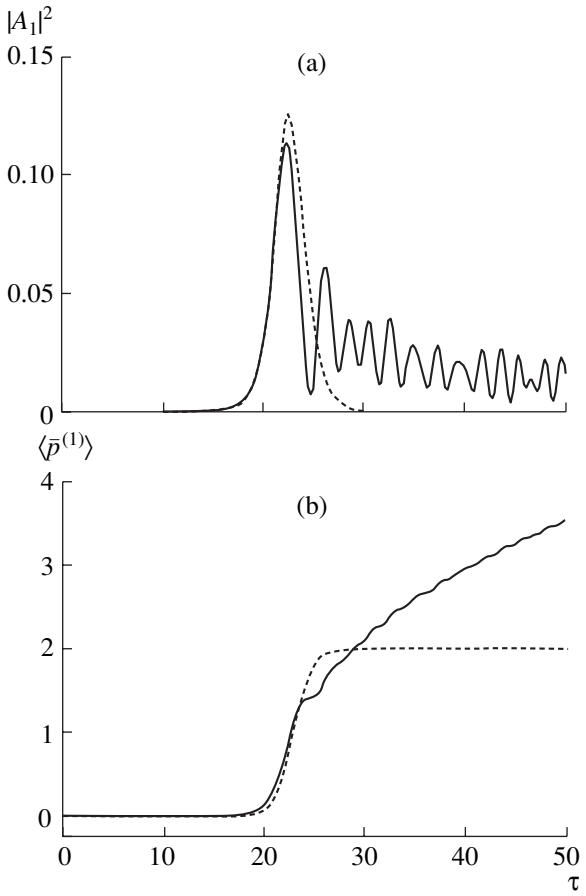

Fig. 2. Semiclassical superradiant regime: $|A_1|^2$ (a) and $\langle \bar{p}^{(1)} \rangle$ (b) vs. τ as obtained from Eqs. (10), (11), and (13) (continuous line) and from the approximated solution (14) and (15) (dashed line), for $\kappa = 2$ and $\delta = 0$.

which can be assumed to be $\sim\sqrt{2/N}$ for a condensate of N atoms. In the linear regime the exponential gain is

$$G = \omega_r\rho\sqrt{2/\kappa} = (3\gamma/2\Delta_0)\sqrt{(I_0 N/m_a\omega)(\lambda^2/A)}, \qquad (16)$$

whereas the peak value of the scattered intensity is

$$I_{\text{peak}} = (\gamma/2\Delta_0)^2[(3/4\pi)(\lambda^2/A)]^2 N^2 I_0, \qquad (17)$$

where $I_0 = (c\epsilon_0/2)|\mathcal{E}_0|^2$ is the pump intensity, A is the cross sectional area of the condensate and $\gamma = \mu^2\omega^3/3\pi c^3\hbar\epsilon_0$ is the natural decay rate of the atomic transition. Figures 2a and 2b show $|A_1|^2$, (a), and $\langle \bar{p}^{(1)} \rangle$, (b), vs. τ as obtained from the numerical solution of Eqs. (10), (11) and (13) (continuous line) and from the approximated solution (14) and (15), for $\kappa = 2$, $A_1(0) = 10^{-4}$ and $b_0 = 1.6 \times 10^{-5}$.

3. QUANTUM MODEL

We proceed now quantizing both the two radiation modes and the center-of-mass motion of the atoms, considering $\theta_j^{(1,2)} = q\hat{\epsilon}_{1,2}\mathbf{x}_j$, $p_j^{(1,2)} \equiv (\rho/2)\bar{p}_j^{(1,2)} = \hat{\epsilon}_{1,2}\mathbf{p}_j/\hbar q$ and $a_{1,2} = (N'\rho/2)^{1/2}\tilde{A}_{1,2}$ as quantum operators satisfying the canonical commutation relations $[\theta_j^{(n)}, p_{j'}^{(n')}] = i\delta_{nn'}\delta_{jj'}$ and $[a_n, a_{n'}^\dagger] = \delta_{nn'}$, with $n, n' = 1, 2$ and $j = 1, \ldots, N'$. In the following, we limit the analysis to a single mode, $n = 1$, and we omit the apices (n) on the variables. With the definitions above, Eqs. (10), (11), and (13), for $\kappa = 0$, are the Heisenberg equations of motion associated with the Hamiltonian:

$$H = \frac{1}{\rho}\sum_{j=1}^{N'} p_j^2 + ig\left(\sum_{j=1}^{N'} a^\dagger e^{i\theta_j} - \text{h.c.}\right) - \delta a^\dagger a = \sum_{j=1}^{N'} H_j(\theta_j, p_j), \tag{18}$$

where $g = \sqrt{\rho/2N'}$. We note that $[H, Q] = 0$, where $Q = a^\dagger a - \sum_{j=1}^{N'} p_j$ is the total atomic momentum exchanged along $\hat{\epsilon}_1$ in units of $\hbar q$. The single-particle Hamiltonian $H(\theta, p)$ in Eq. (18) can be second quantized as

$$\hat{H} = \int_0^{2\pi} d\theta \hat{\Psi}^\dagger(\theta) H\left(\theta, -i\frac{\partial}{\partial\theta}\right)\hat{\Psi}(\theta), \tag{19}$$

where the atomic field operators obey the usual bosonic equal time commutation relations $[\hat{\Psi}(\theta), \hat{\Psi}^\dagger(\theta')] = \delta(\theta - \theta')$ and $[\hat{\Psi}(\theta), \hat{\Psi}(\theta')] = [\hat{\Psi}^\dagger(\theta), \hat{\Psi}^\dagger(\theta')] = 0$ and the normalization condition $\int_0^{2\pi} d\theta \hat{\Psi}(\theta)^\dagger \hat{\Psi}(\theta) = N'$. We introduce creation and annihilation operators for the dimensionless center-of mass operator p, i.e., $\hat{\Psi}(\theta) = \sum_m c_m \langle\theta|m\rangle$, where $p|m\rangle = m|m\rangle$ (with $m = -\infty, \ldots, \infty$) and c_m are bosonic operators obeying the commutation relations $[c_m, c_{m'}^\dagger] = \delta_{mm'}$ and $[c_m, c_{m'}] = 0$. This description of the atomic motion in a BEC assumes that the atoms are unlocalized inside the condensate and that the temperature is so small that the momentum uncertainty $\sigma_{p_{y,z}} \approx \hbar/\sigma_{y,z}$ can be neglected if $\sigma_y \approx W$ and $\sigma_z \approx L$.

It follows from Eq. (19) that the Heisenberg equations for c_m and a are

$$\frac{dc_m}{d\tau} = -i[m^2/\rho - (\delta/N')a^\dagger a]c_m + g(a^\dagger c_{m-1} - a c_{m+1}), \tag{20}$$

$$\frac{da}{d\tau} = i\delta a + g\sum_m c_m^\dagger c_{m-1}. \tag{21}$$

As the bunching term on the right-hand side of the field equation involves the products of creation and annihilation operators, $c_m^\dagger c_{m-1}$, it is useful to introduce the density matrix operator

$$S_{m,n} \equiv \frac{1}{N'} c_m^\dagger c_n e^{-i(m-n)\delta\tau}. \tag{22}$$

A straightforward calculation yields, from Eqs. (20) and (21), the following final set of equations:

$$\frac{dS_{m,n}}{d\tau} = -[i(m-n)\delta_{m,n} + \gamma_{m,n}]S_{m,n} + (\rho/2)[A(S_{m-1,n} - S_{m,n+1}) + A^\dagger(S_{m,n-1} - S_{m+1,n})], \tag{23}$$

$$\frac{dA}{d\tau} = \sum_m S_{m,m-1} - \kappa A, \tag{24}$$

where $\delta_{m,n} = \delta - (m + n)/\rho$ and $A = \sqrt{2/\rho N'}\, a e^{-i\delta\tau}$. We have introduced in the equations two incoherent terms: the term $-\kappa A$, taking into account radiation damping and where κ is defined as in the semiclassical Eq. (13), and a decoherence term for the off-diagonal elements of the density matrix, $-\gamma_{m,n}S_{m,n}$, where $\gamma_{m,n} = (m^2 - n^2)^2(\tau_{dc}/\rho^2)$ and $\tau_{dc} = \omega_r\rho t_{dc}$, where t_{dc} is a time characteristic of the system [18]. An estimate of $\Gamma_{1,0} = \omega_r\rho\gamma_{1,0} = \omega_r^2 t_{dc}$ has been obtained in the MIT experiment both from the linewidth of the Bragg resonance and from the decay of the matter wave [1, 2, 13].

Without the atomic and radiation decay terms, Eqs. (23) and (24) were derived by Moore and coworkers in [9]. However, their analysis was limited to the study of the collective CARL instability and no results were presented for the full nonlinear regime. Preliminary results of numerical and analytical studies of the nonlinear regime described by Eqs. (23) and (24) are contained in [12], whereas perturbative results of the sequential SR scattering, implicitly contained in Eqs. (23) and (24), have been published in [5]. Equations (23) and (24) are the quantum version of the CARL equations (10), (11), and (13) for BECs, where a decoherence mechanism has been added. They determine the temporal evolution of the density matrix elements for the momentum levels. In particular, $p_m = \langle S_{m,m}\rangle$ is the probability of finding the atom in momentum level m, $\langle p\rangle = \sum_m m p_m$ is the average momentum and $\sum_m \langle S_{m,m-1}\rangle$ is the bunching parameter. For a constant field A, Eq. (23) describes the Bragg scattering process, in which $m - n$ photons are absorbed from the pump and scattered into the probe, changing the initial and final momentum states of the atom from m to n.

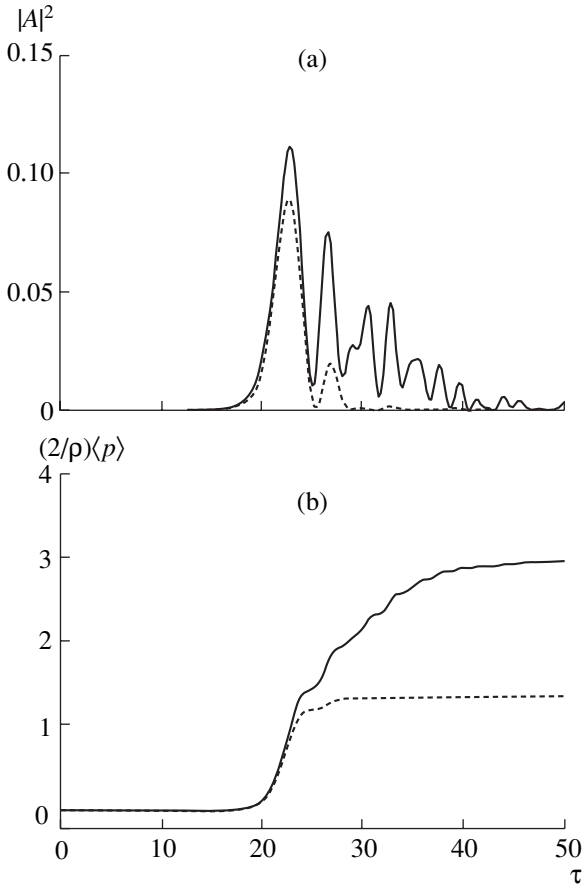

Fig. 3. Semiclassical limit of the quantum model: $|A|^2$ (a) and $(2/\rho)\langle p\rangle$ (b) vs. τ as obtained from Eqs. (23) and (24) for $\kappa = 2$ and $\rho = 10$, $\tau_{dc} = 0$ (continuous line) and $\tau_{dc} = 0.1$ (dashed line).

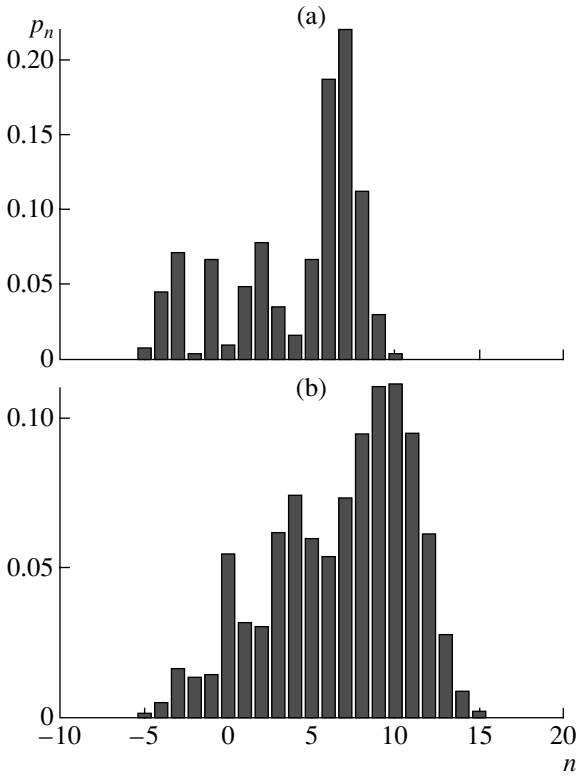

Fig. 4. Momentum population p_n vs. n at the occurring of the first maximum of $|A|^2$ in Fig. 3a, at $\tau = 12.4$ and for $\tau_{dc} = 0$ (a) and at $\tau = 50$ and for $\tau_{dc} = 0.1$ (b).

Conservation of energy and momentum require that during this process $\omega_2 - \omega_1 = (m + n)\omega_r$, i.e., $\delta_{m,n} = 0$. Equations (23) and (24) conserve the norm, i.e., $\sum_m S_{m,m} = 1$, and, when $\kappa = 0$, also the total momentum $Q = (\rho/2)|A|^2 - \langle p\rangle$. In the following, we will investigate only the expectation values of a and $S_{m,n}$ neglecting fluctuations and supposing that $\langle aS_{m,n}\rangle \approx \langle a\rangle\langle S_{m,n}\rangle$. Hence, we will not indicate explicitly the average brackets of the expectation values.

Figures 3a and 3b show $|A|^2$ and $(2/\rho)\langle p\rangle$ vs. τ for $\kappa = 2$, $\rho = 10$, $\delta = 0$, $\tau_{dc} = 0$ (continuous line) and $A(0) = 10^{-4}$, as obtained integrating numerically Eqs. (23) and (24) for the atoms initially in the ground state with $m = 0$, i.e., $S_{m,n}(0) = \delta_{m0}\delta_{n0}$. The dashed line in Fig. 3 shows the effect of the decoherence, for $\tau_{dc} = 0.1$. A comparison with the semiclassical solution of Fig. 2 shows that, for $\rho > \sqrt{\kappa}$, the quantum system behaves, with good approximation, classically. Figure 4a shows the distribution of the population level p_n at the first maximum of the intensity of Fig. 3a, at $\tau = 22.5$, in the case with $\tau_{dc} = 0$. We observe that, at the occurrence of the first superradiant peak of intensity, almost fifteen momentum levels become occupied, with an induced momentum spread comparable to the average momentum. Figure 4b shows the momentum distribution at $\tau = 50$ for $\tau_{dc} = 0.1$ (dashed line in Fig. 3). Decoherence causes the decay of the off-diagonal elements of the density matrix $S_{m,n}$, and, for $\gamma_{m,n}\tau \gg 1$, stops the superradiant emission and makes the momentum distribution stationary and almost symmetric around its average value.

4. QUANTUM EFFECTS IN THE SUPERRADIANT INSTABILITY

Let us now consider the equilibrium state with no field, $A = 0$, and all the atoms in a given momentum state n, i.e., $S_{n,n} = 1$ and the other matrix elements zero. This is equivalent to assume the temperature of the system equal to zero and all the atoms moving with the same momentum $n\hbar\mathbf{q}_1$ without spread. This equilibrium state is unstable for certain values of the detuning δ. In fact, by linearizing Eqs. (23) and (24) around the equilibrium state, the only matrix elements giving linear contributions are $S_{n+1,n}$ and $S_{n,n-1}$, showing that in the linear regime the only transitions allowed from the state n are these towards the levels $n - 1$ and $n + 1$.

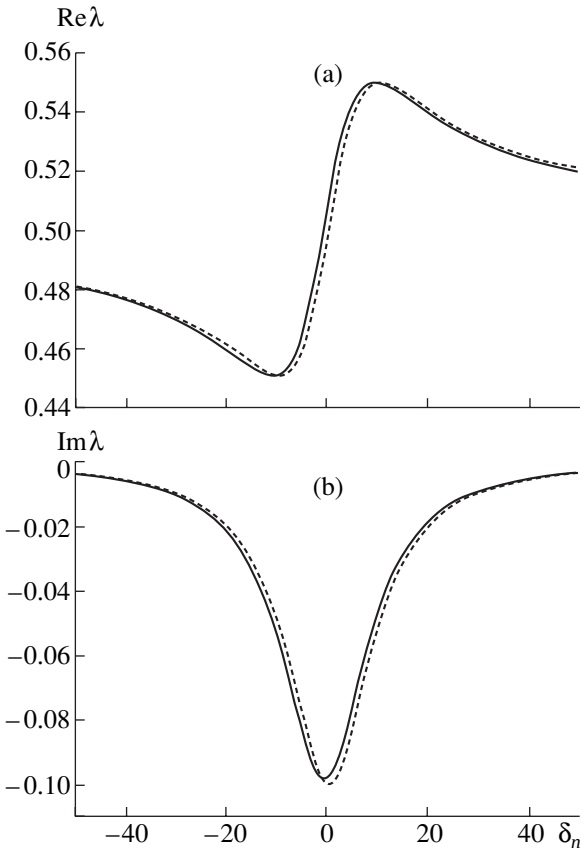

Fig. 5. Reλ (a) and Imλ (b) vs. δ_n, as given by Eqs. (29) and (30) (dashed line), and calculated from the exact solution of Eq. (28) (continuous line) for $\kappa = 10$ and $\rho = 2$.

Introducing the new variables $B_n = S_{n+1,n} + S_{n,n-1}$ and $P_n = S_{n,n-1} - S_{n+1,n}$ and neglecting for sake of simplicity the decoherence term, $-\gamma_{m,n}S_{m,n}$, Eqs. (23) and (24) reduce to the linearized equations:

$$\frac{dB_n}{d\tau} = -i\delta_n B_n - \frac{i}{\rho}P_n, \tag{25}$$

$$\frac{dP_n}{d\tau} = -i\delta_n P_n - \frac{i}{\rho}B_n - \rho A, \tag{26}$$

$$\frac{dA}{d\tau} = B_n - \kappa A, \tag{27}$$

where $\delta_n = \delta - 2n/\rho$. Seeking solutions proportional to $e^{i(\lambda-\delta_n)\tau}$, we obtain the following cubic dispersion relation:

$$(\lambda - \delta_n - i\kappa)(\lambda^2 - 1/\rho^2) + 1 = 0. \tag{28}$$

In the exponential regime, when the unstable (complex) root λ dominates, $B(\tau) \sim e^{i(\lambda-\delta_n)\tau}$ and, from Eq. (25), $P_n \approx -\rho\lambda B_n$. In the SR regime, the semiclassical limit is recovered for $\rho \gg \sqrt{\kappa} > 1$ and $\delta_n \approx \delta$, i.e., neglecting the shift due to the recoil frequency ω_r. In this limit, maximum gain occurs for $\delta = 0$, with $\lambda = -(1+i)/\sqrt{2\kappa}$. Furthermore, $|S_{n,n-1}| \sim |S_{n+1,n}|$, so that the atoms may experience both emission and absorption. This result can be interpreted in terms of single-photon emission and absorption by an atom with initial momentum $n\hbar\mathbf{q}$. In fact, energy and momentum conservation impose $\omega_2 - \omega_1 = (2n \pm 1)\omega_r$ (i.e., $\delta_n = \pm 1/\rho$) when a probe photon is emitted or absorbed, respectively. Because in the semiclassical limit the gain bandwidth is $\Delta\omega \sim \kappa_c \gg \omega_r$ when $\kappa_c > \omega_r\rho$ and $\rho \gg 1$, the atom can both emit or absorb a probe photon. On the contrary, in the quantum limit, the recoil energy $\hbar\omega_r$ can not be neglected, and there is emission without absorption if $|S_{n,n-1}| \ll |S_{n+1,n}|$, i.e., $B_n \approx -P_n$ and $\lambda \approx 1/\rho$. In fact, for $\rho < \sqrt{2\kappa}$, the unstable root $\lambda = \mathrm{Re}\lambda + i\mathrm{Im}\lambda$ can be approximated by

$$\mathrm{Re}\,\lambda \approx \frac{1}{\rho} + \frac{\rho(\delta_n - 1/\rho)/2}{(\delta_n - 1/\rho)^2 + \kappa^2}, \tag{29}$$

$$\mathrm{Im}\,\lambda \approx -\frac{\rho\kappa/2}{(\delta_n - 1/\rho)^2 + \kappa^2}, \tag{30}$$

as shown in Fig. 5, where Reλ (Fig. 5a) and Imλ (Fig. 5b) vs. δ_n, as given by Eqs. (29) and (30) (dashed line), are compared with the exact solution of Eq. (28) (continuous line) for $\kappa = 10$ and $\rho = 2$. Maximum gain, $\mathrm{Im}\lambda \approx -\rho/2\kappa$, occurs for $\delta_n = 1/\rho$ (i.e., $\omega_2 - \omega_1 = (2n+1)\omega_r$) with the same bandwidth $\Delta\omega \sim \kappa_c$ as in the semiclassical limit. However, within the gain bandwidth, $\mathrm{Re}\lambda \approx 1/\rho$ if $\rho \ll \sqrt{2\kappa}$, so that in this limit the gain is due exclusively to emission of photons, contrary to the semiclassical limit where gain is given by the (positive) difference between the emission and absorption average rates. The maximum SR gain in the quantum limit $\rho < \sqrt{2\kappa}$ is then $G = 2(\mathrm{Im}\lambda)\omega_r\rho = \omega_r\rho^2/\kappa = (3/2\pi)\gamma(\Omega_0/2\Delta_0)^2(\lambda^2/A)N'$. We also note the positive slope of the real part of λ in Fig. 5a near resonance, which implies a value of the group velocity $v_g = c/[n + \omega(dn/d\omega)]$ (where $n \approx 1 + (\omega_r/\omega)\rho(\mathrm{Re}\lambda - \delta_n)$ is the index of refraction) smaller than c [13].

5. SEQUENTIAL SUPERRADIANT REGIME

The above results show that the combined effect of the probe and pump fields on a collection of cold atoms in a pure momentum state n is responsible for a collective instability that leads the atoms to populate the adjacent momentum levels $n-1$ and $n+1$. However, in the quantum limit $\rho < \sqrt{2\kappa}$ of the SR regime, $\kappa > 1$ (or in limit $\rho < 1$ of the conservative regime, $\kappa = 0$ [12]) conservation of energy and momentum of the photon constrains the atoms to populate only the upper momentum level $n+1$. This holds also in the nonlinear regime, as

we have verified solving numerically Eqs. (23) and (24). In this quantum limit, the exact equations reduce to those for only three matrix elements, $S_{n,n}$, $S_{n+1,n+1}$, and $S_{n+1,n}$, with $S_{n+1,n+1} + S_{n,n} = 1$. Introducing the new variables $S_n = S_{n+1,n}$ and $W_n = S_{n,n} - S_{n+1,n+1}$, Eqs. (23) and (24) reduce to the well-known Maxwell–Bloch equations for a two-level system [19]:

$$\frac{dS_n}{d\tau} = -[i\delta_n' + \gamma_n]S_n + \frac{\rho}{2}AW_n, \tag{31}$$

$$\frac{dW_n}{d\tau} = -\rho(A^*S_n + \text{h.c.}), \tag{32}$$

$$\frac{dA}{d\tau} = S_n - \kappa A, \tag{33}$$

where $\delta_n' = \delta - (2n+1)/\rho$ and $\gamma_n = (2n+1)^2(\tau_{dc}/\rho^2)$. In the SR regime, for $\kappa > 1$ and $\gamma_n \approx 0$, Eqs. (31)–(33) describe a single collective scattering process in which the atoms, initially in the momentum state n, move to the upper level $n+1$ emitting a π hyperbolic secant pulse, with intensity

$$|A|^2 = \frac{1}{[4(\kappa^2 + \delta_n'^2)]}\,\text{sech}^2[(\tau - \tau_D)/\tau_{SF}] \tag{34}$$

and average momentum

$$\langle p\rangle = n + (1/2)\{1 + \text{Th}[(\tau - \tau_D)/\tau_{SF}]\}, \tag{35}$$

where $\tau_{SR} = 2(\kappa^2 + \delta_n'^2)/\rho\kappa$ is the "superradiant time" [16], $\tau_D = \tau_{SF}\,\text{arcsech}(2|S_n(0)|) \approx -\tau_{SR}\ln\sqrt{2|S_n(0)|}$ is the delay time and $|S_n(0)| \ll 1$ is the initial polarization. Figures 6a and 6b show $|A|^2$ and $\langle p\rangle$ vs. τ calculated solving Eqs. (23) and (24) numerically with $\kappa = 10$, $\rho = 2$, $\delta = 0.5$, $\tau_{dc} = 0$ (solid line) and $\tau_{dc} = 0.005$ (dashed line), with the same initial conditions as in Fig. 3. We observe a sequential SR scattering, in which the atoms, initially in the level $n = 0$, change their momentum by discrete steps of $\hbar\mathbf{q}$ and emit a SR pulse during each scattering process. We observe that for $\delta = 1/\rho$ the field is resonant only with the first transition, from $n = 0$ to $n = 1$; for a generic initial state n, resonance occurs when $\delta = (1 + 2n)/\rho$, so that in the case of Fig. 6a (solid line) the peak intensity of successive SR pulses is reduced (by the factor $1/[\kappa^2 + (2n/\rho)^2]$) whereas the duration and the delay of the pulse are increased. However, the pulse retains the characteristic sech^2 shape and the area remains equal to π, inducing the atoms to increase their momentum by the finite value $\hbar\mathbf{q}$ along the direction $\hat{\epsilon}_1$. We note that, although the SR time in the quantum limit ($\tau_{SR} = 2\kappa/\rho$ at resonance) can be considerable longer than the characteristic SR time obtained in the classical limit, $\tau_{SR}^{(c)} = \sqrt{2\kappa}$, the peak intensity of the pulse in the quantum limit is approximately half of the value obtained in the semiclassical limit.

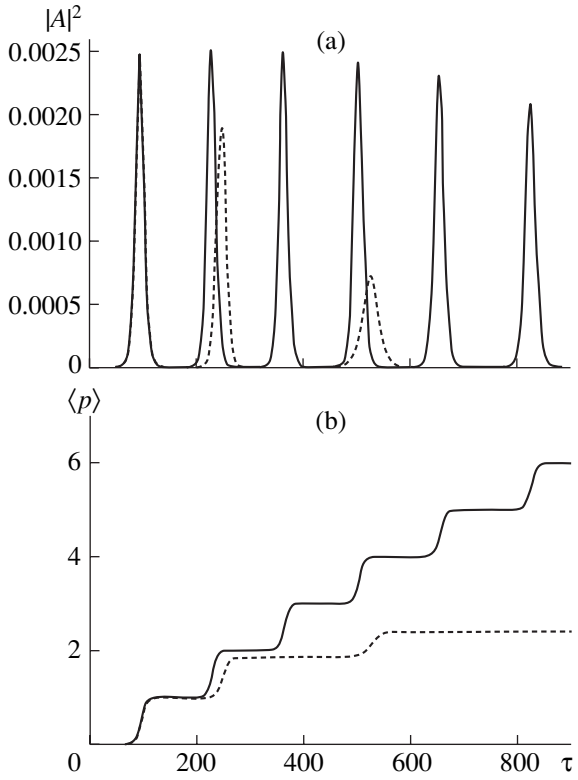

Fig. 6. Sequential superradiant regime: (a) $|A|^2$ and (b) $\langle p\rangle$ vs. τ, for $\rho = 2$, $\delta = 0.5$, $\kappa = 10$, $\tau_{dc} = 0$ (continuous line) and $\tau_{dc} = 0.005$ (dashed line).

Finally, we observe that decoherence inhibits the observation of the sequential SR scattering, as shown by the solution of Fig. 6 obtained for $\tau_{dc} = 0.005$ (dashed line). The number n of observable SR pulses can be estimated assuming $\gamma_n\tau_{SR} < 1$, which gives $2n + 1 < \sqrt{\rho^3/2\kappa\tau_{dc}}$. For the case of Fig. 6, $n < 4$.

6. COMPARISON WITH THE MIT EXPERIMENT

In the MIT experiment [1], a sodium BEC was exposed to a single off-resonant laser pulse red-detuned by $\Delta_0/2\pi = 1.7$ GHz from the $^3S_{1/2} \longrightarrow {}^3P_{3/2}$ transition, with $\lambda = 589$ nm, natural width $\gamma = 0.62 \times 10^8$ s^{-1} and recoil frequency $\omega_r = 3 \times 10^5$ s^{-1}. The condensate had a cigar-shaped form, 20 μm in diameter and 200 μm in length, containing approximately $N = 10^6$ atoms. Assuming that $N' = N/2$ atoms participate in each of two superradiant emissions along the main axis of the condensate, the dimensionless parameters are $\rho \approx 44 I_0^{1/3}$ and $\kappa \approx 5.5 \times 10^4 I_0^{-1/3}$, where I_0 is the pump intensity in mW/cm^2. Because typical laser intensities were between 1 and 100 mW/cm^2, $\rho/\sqrt{2\kappa} \approx 0.13\sqrt{I_0} \leq$

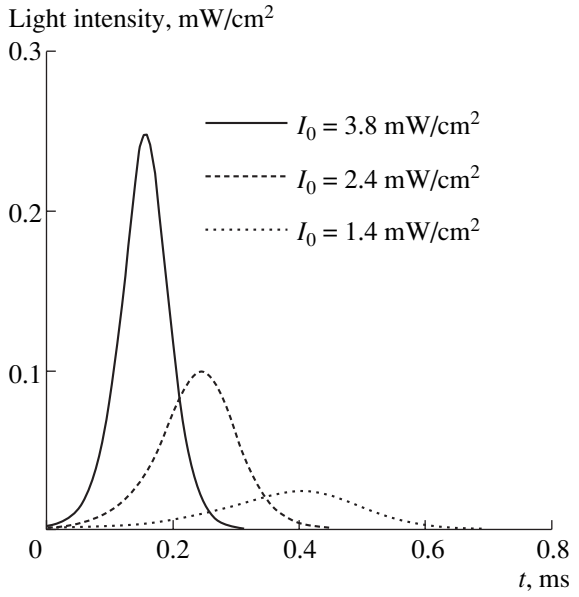

Fig. 7. Temporal evolution of the scattered intensity as given by the approximate formula (36), for the MIT experiment and three different values of the incident intensity, 3.8 (solid line), 2.4 (dashed line) and 1.4 mW/cm^2 (dotted line).

1, so that the quantum model must be used. The decoherence rate has been measured in [1] by Bragg spectroscopy as $2\Gamma_{1,0} \approx (2\pi)5$ kHz, giving the dimensionless coherence time $\tau_{dc} \approx 0.35 I_0^{1/3}$. The superradiant gain is approximately $G \approx 11 I_0$, where G is given in ms^{-1}, whereas the first pulse delay is about $t_D \approx \ln(N)/2G \approx (0.6/I_0)$ ms, in good agreement with the measured values. Furthermore, an estimate of the number of observable sequential scattering processes can be obtained from the condition $\gamma_n \tau_{SR} < 1$, which gives $2n + 1 < 0.7\sqrt{I_0}$. For $n = 0$, the intensity threshold for superradiance is $I_0 \approx 2$ mW/cm^2, whereas for the second and third sequential scattering ($n = 1, 2$) is $I_0 \approx 18$ mW/cm^2 and $I_0 \approx 50$ mW/cm^2, respectively. Figure 7 shows the temporal evolution of the light intensity observed in the MIT experiment for laser intensities I_0 equal to 3.8 (solid line), 2.4 (dashed line) and 1.4 (dotted line) mW/cm^2, as given by Eq. (34), conveniently written as

$$I(t) = 0.146 I_0 e^{-31.4t} \mathrm{sech}^2[5.53 I_0 (t - 0.62/I_0)], \quad (36)$$

where I and I_0 are given in mW/cm^2 and t in ms, and where we added a decoherence damping factor with a decoherence time of 32 μs.

In the quantum limit, SR emission parallel and antiparallel to the $\hat{z}$ axis induces in the atoms a recoil momentum $\mathbf{p} = \hbar q[n_1 \hat{\epsilon}_1 + n_2 \hat{\epsilon}_2]$, with $n_{1,2}$ integers. We assumed the existence of two distinct classes of atoms interacting with the two independent SR pulses separately.

The first SR scattering generates two condensates of approximately $N/2$ atoms moving with momentum $\mathbf{p}_{1,2} = \hbar q \hat{\epsilon}_{1,2}$, i.e., with (n_1, n_2) equal to (1, 0) and (0,1), at an angle of 45° with respect to the z-axis. Our model assumes that the two atomic families remain independent, the first recoiling along $\hat{\epsilon}_1$, i.e., with $(n_1, 0)$, and the second along $\hat{\epsilon}_2$, with $(0, n_2)$. However, at the second scattering, nothing prevents the atoms in the first (second) family from recoiling along the other direction $\hat{\epsilon}_2$ ($\hat{\epsilon}_1$), producing the orders (2, 0), (0, 2) (with $N/4$ atoms) and (1, 1) (with $N/2$ atoms). In a similar way, the third scattering produces the orders (3, 0), (0, 3) (with $N/8$ atoms) and (2, 1), (1, 2) (with $(3/8)N$ atoms). This atomic distribution has been clearly observed in the MIT experiment, after increasing the exposure time to the laser source and letting the atomic cloud expand ballistically after the interaction. In particular, the images of the atomic clouds corresponding to the orders (1, 0), (0, 1) and (1, 1) appear to have the same density (with $N/2$ atoms). The extremely small decoherence of the system in the MIT experiment allows the atoms to emit up to three sequential superradiantly scattered pulses.

7. CONCLUSIONS

In conclusion, we have presented a theory describing the atomic motion and its effects upon superradiant Rayleigh scattering from Bose–Einstein condensates. Initially, the atomic motion is treated classically, and the mean features of the superradiant regime are discussed. Then, the semiclassical model is extended including a quantum mechanical description of the atomic motion. We have discussed the quantum limit in which the atomic momentum changes by discrete units of the photon recoil momentum $\hbar\mathbf{q}$. In this limit, the exact equations reduce, for each sequential scattering, to the Maxwell–Bloch equations for two momentum levels. These results show that the regular atomic momenta distribution observed in the MIT experiment [1] can be interpreted as being due to sequential superradiant scattering, as originally proposed in [1] and investigated in detail in [5]. Conversely, the quantum nature of the atomic motion in a BEC may be neglected in the high density limit (i.e., for $\rho \gg \sqrt{\kappa}$).

We finally comment the differences between our results and these of [4, 5]. Our theory extends the model of [4] taking into account (although for only a single mode) all the high-order "side modes" n, corresponding to multiple scattering of the pump photons. The authors of [4] study the exponential build-up of the first-order side modes, (1, 0) and (0, 1), starting from quantum fluctuation. We obtain the same gain as in [4] in the limit $\rho < \sqrt{\kappa}$, and the semiclassical superradiant gain

in the opposite limit. Furthermore, in [4] the nonlinear effects are considered introducing the population depletion of the momentum ground state (0, 0), whereas the authors of [5] extend the nonlinear analysis including the second-order mode (1, 1). Then, the authors implement their model adding three phenomenological decay terms to the reduced equations, i.e., a radiation loss term $-\kappa_c I$ (where I is the scattered intensity), a dephasing term equivalent to $-\gamma_\perp S_{1,0}$ and a decay term of the population level $n = 1$ due to coupling with excluded levels, equivalent to $-\mathcal{L}S_{1,1}$. We note that we do not need this last term because we consider all the momentum levels. Then, the authors compare their model with the MIT experiment integrating numerically the equations with $\kappa_c = \mathcal{L} \sim \gamma_\perp \sim 10^5$ s^{-1}. This choice of parameters strongly disagrees with our assumption that $\kappa_c = c/L \sim 10^{13}$ s^{-1} and with the usual condition for observing superradiance, i.e., $\kappa \gg \gamma_\perp$. The agreement of our model with the experimental results, as shown in Fig. 7, seems to confirm the correctness of our model against the model of [5]. However, a detailed comparison of high-order sequential superradiant scattering observed in the MIT experiment should require a full bidimensional analysis of the atomic motion coupled with two scattered fields, that will be the object of a future investigation.

REFERENCES

1. Inouye, S., Chikkatur, A.P., Stamper-Kurn, D.M., Stenger, J., Pritchard, D.E., and Ketterle, W., 1999, *Science*, **285**, 571.
2. Inouye, S., Pfau, T., Gupta, S., Chikkatur, A.P., Görlitz, A., Pritchard, D.E., and Ketterle, W., 1999, *Nature*, **402**, 641.
3. Mikio Kozuma, Yoichi Suzuki, Yoshio Torii, Toshiaki Sugiura, Takahiro Kugam, Hagley, E.W., and Deng, L., 1999, *Science*, **286**, 2309.
4. Moore, M.G. and Meystre, P., 1999, *Phys. Rev. Lett.*, **83**, 5202.
5. Mustecaplioglu, O.E. and You, L., 2000, *Phys. Rev. A*, **62**, 063615.
6. Bonifacio, R., De Salvo Souza, L., Narducci, L.M., and D'Angelo, E.J., 1994, *Phys. Rev. A*, **50**, 1716.
7. Bonifacio, R. and De Salvo, L., 1995, *Appl. Phys. B*, **60**, S233.
8. Bonifacio, R., Robb, G.R.M., and McNeil, B.W.J., 1997, *Phys. Rev. A*, **56**, 912.
9. Moore, M.G. and Meystre, P., 1998, *Phys. Rev. A*, **58**, 3248.
10. Moore, M.G., Zobay, O., and Meystre, P., 1999, *Phys. Rev. A*, **60**, 1491.
11. Piovella, N., Bonifacio, R., McNeil, B.W.J., and Robb, G.R.M., 2001, *Opt. Commun.*, **187**, 165.
12. Piovella, N., Gatelli, M., and Bonifacio, R., 2001, *Opt. Commun.*, **194**, 167.
13. Inouye, S., Low, R.F., Gupta, S., Pfau, T., Gorlitz, A., Gustavson, T.L., Pritchard, D.E., and Ketterle, W., 2000, *Phys. Rev. Lett.*, **85**, 4225.
14. Bonifacio, R., Pellegrini, C., and Narducci, L.M., 1984, *Opt. Commun.*, **50**, 373.
15. Bonifacio, R., De Salvo Souza, L., Pierini, P., and Piovella, N., 1990, *Nucl. Instrum. Methods Phys. Res. A*, **296**, 358.
16. Bonifacio, R., Schwendimann, P., and Haake, F., 1971, *Phys. Rev. A*, **4**, 302; Bonifacio, R. and Lugiato, L.A., 1975, *Phys. Rev. A*, **11**, 1507.
17. Bonifacio, R. and Casagrande, F., 1985, *J. Opt. Soc. Am. B*, **2**, 250.
18. Bonifacio, R., Olivares, S., Tombesi, P., and Vitali, D., 2000, *Phys. Rev. A*, **61**, 5382.
19. Arecchi, F.T. and Bonifacio, R., 1965, *IEEE J. Quantum Electron.*, **1**, 169.